

---

# Was Residual Penalty and Neural Operators All We Needed for Solving Optimal Control Problems?

---

**Oliver G. S. Lundqvist**

Department of Mathematics and Systems Analysis  
Aalto University, Espoo, Finland  
oliver.lundqvist@aalto.fi

**Fabricio Oliveira**

Department of Mathematics and Systems Analysis  
Aalto University, Espoo, Finland  
fabricio.oliveira@aalto.fi

## Abstract

Neural networks have been used to solve optimal control problems, typically by training neural networks using a combined loss function that considers data, differential equation residuals, and objective costs. We show that including cost functions in the training process is unnecessary, advocating for a simpler architecture and streamlined approach by decoupling the optimal control problem from the training process. Thus, our work shows that a simple neural operator architecture, such as DeepONet, coupled with an unconstrained optimization routine, can solve multiple optimal control problems with a single physics-informed training phase and a subsequent optimization phase. We achieve this by adding a penalty term based on the differential equation residual to the cost function and computing gradients with respect to the control using automatic differentiation through the trained neural operator within an iterative optimization routine. We showcase our method on nine distinct optimal control problems by training three separate DeepONet models, each corresponding to a different differential equation. For each model, we solve three problems with varying cost functions, demonstrating accurate and consistent performance across all cases.

## 1 Introduction

An *optimal control problem* is an optimization problem in which the system dynamics are described by differential equations, either ordinary differential equations (ODEs) or partial differential equations (PDEs), that explicitly depends on a control input. These problems arise across a wide range of practical applications, including power plant operation [1, 2, 3], flight trajectory optimization [4, 5, 6], control of biological systems [7, 8], and economic decision-making in areas such as investment and trading [9, 10].

Traditional numerical approaches to optimal control problems are computationally intensive, making neural networks an attractive alternative. As such, recent studies have explored physics-informed neural networks (PINNs) and neural operators (NOs) for solving optimal control problems [11, 12, 13, 14, 15], particularly when the constraints are complex, nonlinear PDEs. Existing neural network models are typically trained for a single task, requiring retraining if problem parameters or cost functions change. For example, in a tracking problem, the tracked target may change, leading to a corresponding change in the cost function. In flight control, the objective may vary depending on the mission phase, such as achieving the fastest climb, the most economical cruise, or the safest landing,

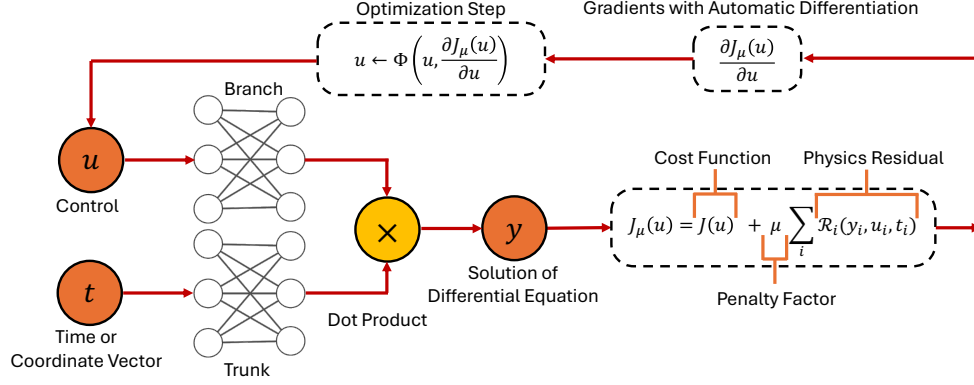


Figure 1: The schematic of our proposed method.

each defining a different optimal control problem. Similarly, operating a power plant involves distinct objectives during startup, steady-state operation, and shutdown, resulting in various formulations of the cost function depending on the operational context.

To address this limitation, we propose a method that fully decouples neural network training from the optimal control problem, eliminating the need for retraining when cost functions or parameters change. Our approach trains a single NO in advance, allowing it to solve multiple optimal control problems efficiently. Moreover, since neural network inference is fast from a computational perspective, we claim that our method is also suitable for real-time applications. Additionally, we argue that solving a complex optimal control problem is fundamentally equivalent to training a well-generalizable physics-informed NO, making specialized architectures unnecessary. In line with Occam’s razor, we advocate for simpler and less complex architectures, as our results demonstrate that such models are sufficient for solving a wide range of control problems without the need for elaborate or highly specialized designs. In addition, our approach broadens the original scope of NOs beyond their typical use as solvers for differential equations, thus showcasing a valuable discovery of their capabilities.

Our method employs a direct optimization approach, integrating automatic differentiation with nonlinear programming to efficiently compute control gradients while enforcing differential equation constraints through residual penalties. A schematic representation of our approach is shown in Figure 1. We focus on the DeepONet architecture, comparing optimization routines such as gradient descent (GD), adaptive moment estimation (ADAM) [16], and Broyden–Fletcher–Goldfarb–Shanno (BFGS) [17] across multiple optimal control problems. We note that, although we use DeepONet, our approach is not limited to this architecture, leaving exploration of alternatives for future work.

Our main contributions are as follows. We demonstrate that a single NO can be reused with our method across multiple optimal control problems, eliminating the need for retraining, thereby enabling their use in practical settings. We further demonstrate that training a NO alone is sufficient for solving optimal control problems, reducing the need for complex architectural modifications. This suggests that, in many cases, specialized control networks may not be necessary, offering a more streamlined approach for using neural networks with optimal control problems. Our approach is both simple and powerful, showcasing the versatility of NOs in solving a broad range of problems beyond their original task.

The rest of this paper is structured as follows: Section 2 reviews related work. Section 3 introduces our direct method. Section 4 presents experimental results on three different DeepONet models, each solves three different optimal control problems. Section 5 concludes the study.

## 2 Related Work

In recent years, PINNs have been widely used to solve differential equations [18, 19, 20, 21, 22]. An extension of PINNs for solving optimization problems was performed by Lu et al. [23], where the authors used a PINN and a control network for topology optimization for inverse design problems. They trained a neural network on a common loss function consisting of the residual of the differential

equation and the cost function of the topology optimization problem. Molawi et al. [11] extended the idea of a control neural network and a PINN to optimal control problems. Song et al. [15] split the control term into two variables, dividing the training loss into a differential equation term and a regularizing term describing the cost, and used an alternating direction method of multipliers for training the neural networks. Similarly, [24, 13, 14] have explored the use of two (or more) neural network models, PINNs and a control neural network, to solve optimal control problems.

Another common approach is to utilize the adjoint state equation, which arises from Pontryagin’s Minimum Principle [25] together with PINNs. Employing Pontryagin’s Minimum Principle transforms the optimal control problem into a set of differential equations defined by the Hamiltonian of the system and adjoint state equations. Yin et al. [26] used a direct adjoint looping approach to solve the optimal control problem by using two separate neural networks to solve it, one for the differential equation and one for the adjoint equation that arises from Pontryagin’s Minimum Principle. Schiassi et al. [27] also used Pontryagin’s Minimum Principle and trained a PINN for solving the two-point boundary value problem for a quadratic cost function directly. Demo et al. [24] used a PINN and a control network in sequence, where the output of the PINN was given as input to the control network, which solved for the adjoint equation and derived the optimal control. These methods showed promising results on their respective test problems, but are only capable of solving the particular optimal control problem (i.e., with fixed cost function parameterization) for which the neural networks were trained.

Physics-informed NOs have also been applied to solve optimal control problems [28, 29, 30]. Hwang et al. [31] showed how a modified DeepONet can be used to solve optimal control problems by first training a model and thereafter searching for the optimal control by using nonlinear programming and unconstrained optimization routines, where the gradients of the cost function were calculated by automatic differentiation with respect to the control. The approach in [31] is similar to our proposed idea, however, the authors used an autoencoder to reconstruct the control function before re-feeding it to the NO model in the optimization routine’s iterations. In contrast, we show how this can be done without an autoencoder by properly penalizing the cost function with the physics residual, thus avoiding any increased complexity in the network architecture and associated more computationally expensive training process.

### 3 Methodology

Here we define the preliminaries of NOs and optimal control problems, followed by our methodology for using NOs in what we refer to as the *direct* optimization of such problems.

#### 3.1 Neural Operators

Consider the following general ordinary time-dependent differential equation

$$\begin{aligned}\dot{\mathbf{y}}(t) &= \mathbf{f}(\mathbf{y}(t), \mathbf{u}(t), t), \\ \mathbf{y}(0) &= \mathbf{y}_0,\end{aligned}\tag{1}$$

where  $\mathbf{y}(t) \in \mathbb{R}^n$  denotes the *state* at time  $t \in [0, T]$ , and  $\mathbf{u}(t) \in \mathcal{U} \subset C^\infty([0, T])^n$  denotes the *control* function. The dynamics of the system are described with  $\mathbf{f} : \mathbb{R}^n \times \mathcal{U} \times [0, T] \rightarrow \mathbb{R}^n$ . The initial state is given as  $\mathbf{y}_0 \in \mathbb{R}^n$ . Without loss of generality, our presentation considers only ODE systems and no spatial variables. However, we note that our developments can easily be extended to consider PDEs and spatial coordinates since NOs are capable of solving both ODEs and PDEs, as we show in our experiments in section 4. To ease the notation, we omit the arguments, for example, by denoting  $\mathbf{u}(t) := \mathbf{u}$ , only including them when the context requires. In addition, boldfaced variables represent vectors, while nonboldfaced variables are scalars.

We define  $\tilde{\mathbf{y}}$  as the *solution* of (1). We seek to find an operator  $\mathcal{G} : \mathcal{U} \times [0, T] \rightarrow \mathbb{R}^n$  that solves the differential equation (1) for any given function  $\mathbf{u}$ . Hence, we write the *operator* as

$$\mathcal{G}(\mathbf{u})(t) = \tilde{\mathbf{y}}.\tag{2}$$

A *Neural Operator* approximates operator  $\mathcal{G}$  with a neural network. Lu Lu et al. [32] presented an architecture, the *Deep Operator Network* (DeepONet), based on the universal approximation theorem for operators [33]. The basic architecture consists of two parallel networks called *branch* and *trunk*.

The branch network receives as input the function  $\mathbf{u}$  discretized into  $m$  points called *sensor locations*, thus denoted by the vector  $\{\mathbf{u}_k\}_{k=0}^{m-1} \in \mathbb{R}^{n \times m}$ . Respectively, the trunk network receives discrete times  $t_i$  for some  $i$ -discretization of time. Both the trunk and branch networks are fully connected networks in their simplest form. At the end of the DeepONet, the outputs of the trunk and branch network are combined with a dot product. Generally, a NO seeks to simultaneously approximate the operator  $\mathcal{G}$  and solve the differential equation (1). We define the NO  $\mathcal{G}_\theta : \mathbb{R}^{n \times m} \times [0, T] \rightarrow \mathbb{R}^n$  with parameters  $\theta$  and at time point  $t_i$  as

$$\mathcal{G}_\theta(\{\mathbf{u}_k\}_{k=0}^{m-1})(t_i) \approx \tilde{\mathbf{y}}(t_i). \quad (3)$$

In practice, multiple time points  $\{t_i\}$  can be input as a batch for efficient evaluation, but we omit this in the notation for clarity. For more details of the DeepONet architecture, technical details, and its variants, we refer the reader to [32, 34, 35, 36].

### 3.2 A Direct Method for Optimal Control Problems

A typical optimal control problem can be defined as

$$\begin{aligned} \min_{\mathbf{u}} J(\mathbf{u}) &= \min_{\mathbf{u}} \int_0^T L(\mathbf{y}, \mathbf{u}, t) dt + E(\mathbf{y}(T), \mathbf{u}(T)) \\ \text{s.t. } \dot{\mathbf{y}} &= \mathbf{f}(\mathbf{y}, \mathbf{u}, t), \quad \mathbf{y}(0) = \mathbf{y}_0, \end{aligned} \quad (4)$$

where  $L$  is the running cost and is a smooth function with the mapping  $L : \mathbb{R}^n \times \mathcal{U} \times [0, T] \rightarrow \mathbb{R}$ , and  $E$  is the terminal cost with mapping  $E : \mathbb{R}^n \times \mathcal{U} \rightarrow \mathbb{R}$ . The constraint equation  $\dot{\mathbf{y}} = \mathbf{f}(\mathbf{y}, \mathbf{u}, t)$  is a set of ordinary differential equations with initial conditions  $\mathbf{y}(0) = \mathbf{y}_0$ . The objective is to find a control  $\mathbf{u}$  that minimizes the cost function  $J(\mathbf{u})$ .

For solving (4), one can resort to the *indirect methods* using Pontryagin's Minimum Principle [25] and transfer the problem to a two-point boundary value problem, which can be solved with, for example, shooting methods [37]. Another approach is the *direct method*, which discretizes the optimal control problem and treats it as a nonlinear programming (NLP) problem [38]. This can be achieved by discretizing the time  $t$  as  $t_i = i\Delta t$ ,  $i = 0, 1, 2, \dots, I-1$ , where  $\Delta t$  is the respective discretization step. The corresponding discrete approximations of the functions are denoted as  $\mathbf{y}_i = \mathbf{y}(t_i)$  and  $\mathbf{u}_i = \mathbf{u}(t_i)$ . This reformulation allows the continuous optimal control problem (4) to be transformed into its discrete counterpart

$$\begin{aligned} \min_{\{\mathbf{u}_i\}_{i=0}^{I-1}} \bar{J}(\{\mathbf{u}_i\}_{i=0}^{I-1}) &= \min_{\{\mathbf{u}_i\}_{i=0}^{I-1}} \sum_{i=0}^{I-1} L(\mathbf{y}_i, \mathbf{u}_i, t_i) \Delta t + E(\mathbf{y}_{I-1}, \mathbf{u}_{I-1}) \\ \text{s.t. } \dot{\mathbf{y}}_i(t) &= \mathbf{f}(\mathbf{y}_i, \mathbf{u}_i, t_i), \quad \forall i = 0 \dots I-1, \\ \mathbf{y}_0 &= \mathbf{y}_0, \end{aligned} \quad (5)$$

making it suitable for numerical computations. Here, we have replaced the continuous integral with a summation for simpler notation, but in practice, an integration rule would be used, for example, trapezoidal integration. Equation (5) is now an NLP problem. In general, solving NLP problems require the computation of gradients of the cost function  $\bar{J}(\mathbf{u}_i)$  with respect to  $\mathbf{u}_i$ , i.e.,  $\partial \bar{J}(\mathbf{u}_i) / \partial \mathbf{u}_i$  and, thus, solving a discretized optimal control problem is not trivial. Similarly, higher-order methods, such as Newton's method, would need to compute the Hessian  $\partial^2 \bar{J}(\mathbf{u}_i) / \partial \mathbf{u}_i^2$  or its approximations. Fortunately, neural networks are a suitable surrogate in settings where one needs to compute gradients, as neural networks are differentiable by automatic differentiation with respect to the input. Next, we show how this can be used to our benefit.

### 3.3 Neural Operators for Direct Methods

The discretized optimal control problem (5) can be solved as an NLP problem with NOs acting as a surrogate for the differential equation constraints. That is, we replace the differential equations in the constraints of (5) with our pre-trained NO. To ensure that the integrals in the cost function are evaluated without the need for interpolation, the time discretization points  $t_i$  are chosen to coincide with the sensor locations  $\mathbf{u}_i$ . This leads to the following formulation:

$$\begin{aligned} \min_{\{\mathbf{u}_i\}_{i=0}^{I-1}} \bar{J}(\{\mathbf{u}_i\}_{i=0}^{I-1}) &= \min_{\{\mathbf{u}_i\}_{i=0}^{I-1}} \sum_{i=0}^{I-1} L(\mathbf{y}_i, \mathbf{u}_i, t_i) \Delta t + E(\mathbf{y}_{I-1}, \mathbf{u}_{I-1}) \\ \text{s.t. } \mathcal{G}_\theta(\{\mathbf{u}_k\}_{k=0}^{I-1})(t_i) &= \mathbf{y}_i, \quad \forall i = 0, \dots, I-1. \end{aligned} \quad (6)$$

Since  $\mathcal{G}_\theta$  is a neural network (a NO), the output of the neural network can be differentiated with respect to the input, thus, an optimization routine for NLP problems, such as GD, can be employed to solve the problem. For that, we require only two things. First, the NO must be trained, generalizable, and expressive enough to have a wide enough search space. This can be ensured in practice by making the number of functions in the NO training set large enough. Second, since we want to optimize on the control (input)  $\mathbf{u}$  and repeatedly update  $\mathbf{u}$ , the NO can produce solutions  $\mathbf{y}$  that do not approximate the solution to the differential equation. To address this, the cost function must be properly penalized with the residual of the differential equation, ensuring that the control remains in the known search space and satisfies the differential equation. Therefore, we define the *residual*,  $\mathcal{R}_i$ , of the discretized differential equation as

$$\mathcal{R}_i(\mathbf{f}, \mathbf{y}_i, \mathbf{u}_i, t_i) = \|\dot{\mathbf{y}}_i - \mathbf{f}(\mathbf{y}_i, \mathbf{u}_i, t_i)\|_2^2, \quad (7)$$

which can be computed with automatic differentiation in a standard physics-informed way. We thereafter penalize the cost function (6) with the differential equation residual (7), obtaining

$$\begin{aligned} \min_{\{\mathbf{u}_i\}_{i=0}^{I-1}} \bar{J}_\mu(\{\mathbf{u}_i\}_{i=0}^{I-1}) &= \min_{\{\mathbf{u}_i\}_{i=0}^{I-1}} \sum_{i=0}^{I-1} L(\mathbf{y}_i, \mathbf{u}_i, t_i) \Delta t + E(\mathbf{y}_{I-1}, \mathbf{u}_{I-1}) \\ &\quad + \frac{\mu}{I} \sum_{i=0}^{I-1} \mathcal{R}_i(\mathbf{f}, \mathbf{y}_i, \mathbf{u}_i, t_i) \\ \text{s.t. } \mathcal{G}_\theta(\{\mathbf{u}_k\}_{k=0}^{I-1})(t_i) &= \mathbf{y}_i \quad \forall i = 0, \dots, I-1, \end{aligned} \quad (8)$$

where  $\mu \in \mathbb{R}^+$  is a *penalty* factor. Given a sufficiently large penalty factor, this enforces the optimization routine to remain within the domain where the residuals of the differential equation remain small. The penalized cost function  $\bar{J}_\mu$  is differentiable with respect to the control  $\mathbf{u}$  at sensor locations  $k$  since the differential equation was replaced with the NO  $\mathcal{G}_\theta$ . The differentiability of the cost function with respect to  $\mathbf{u}$  allows us to use any optimization routine that utilizes gradients of the penalized cost function. We summarize the solution process in Algorithm 1, where  $\mathbf{u}_i \leftarrow \Phi(\mathbf{u}_i, \frac{d\bar{J}_\mu}{d\mathbf{u}_i})$  represents the current solution update step performed (e.g., a step in the gradient direction for GD) within the optimization routine. We denote automatic differentiation as *AutoDiff*.

---

**Algorithm 1** Gradient-based Optimization using a Neural Operator

---

- 1: **Input:** Pre-trained Neural Operator  $\mathcal{G}_\theta$ ; discretized cost function  $\bar{J}(\mathbf{u})$
  - 2: **Output:** Optimal control  $\mathbf{u}^*$
  - 3: **Initialize:** Discretized control  $\{\mathbf{u}_i\}_{i=0}^{I-1}$  with an initial guess (e.g., zero); define  $t_i = i\Delta t$  to match  $\mathbf{u}_i \equiv \mathbf{u}(t_i)$
  - 4: **while** not converged **do**
  - 5:      $\mathbf{y}_i = \mathcal{G}_\theta(\{\mathbf{u}_k\}_{k=0}^{I-1})(t_i) \quad \forall i = 0, \dots, I-1$  ▷ Forward pass
  - 6:      $\dot{\mathbf{y}}_i = \frac{d}{dt} \mathcal{G}_\theta(\{\mathbf{u}_k\}_{k=0}^{I-1})(t_i) \quad \forall i = 0, \dots, I-1$  ▷ Time derivative via AutoDiff
  - 7:      $\mathcal{R}_i = \|\dot{\mathbf{y}}_i - \mathbf{f}(\mathbf{y}_i, \mathbf{u}_i, t_i)\|_2^2 \quad \forall i = 0, \dots, I-1$  ▷ Residuals
  - 8:      $\bar{J}_\mu(\{\mathbf{u}_i\}_{i=0}^{I-1}) = \bar{J}(\{\mathbf{u}_i\}_{i=0}^{I-1}) + \frac{\mu}{I} \sum_{i=0}^{I-1} \mathcal{R}_i$  ▷ Penalized cost
  - 9:     Compute  $\frac{d\bar{J}_\mu}{d\mathbf{u}_i} \quad \forall i = 0, \dots, I-1$  ▷ Gradients via AutoDiff
  - 10:      $\mathbf{u}_i \leftarrow \Phi(\mathbf{u}_i, \frac{d\bar{J}_\mu}{d\mathbf{u}_i}) \quad \forall i = 0, \dots, I-1$  ▷ Update step
  - 11: **end while**
  - 12: **return**  $\mathbf{u}^* \leftarrow \{\mathbf{u}_i\}_{i=0}^{I-1}$
- 

## 4 Experiments

We conduct three different experiments by training three different DeepONet models for nine optimal control problems, i.e., three problems for each model, demonstrating our proposed method’s re-usability, how it extends the original scope of NOs, and its architectural simplicity. The models are used for solving the discretized optimal control problem (8) by our method in Algorithm 1. The experiments are conducted in two steps. First, the DeepONet models are trained purely as physics-informed, that is, we do not use any true solution data of the differential equations for training

the models. Then, we use each trained model for three optimal control problems with different cost functions  $J(\mathbf{u})$ .

#### 4.1 Experimental Setup

**Differential Equations.** We consider the following differential equations and naming of the optimal control problems:

$$\begin{aligned}
\text{Linear ODE : } & \dot{y}(t) = -y(t) + u(t) \\
& y(0) = 1, \quad t \in [0, 1] \\
\text{Nonlinear ODE : } & \dot{y}(t) = \frac{5}{2}(-y(t) + y(t)u(t) - u(t)^2) \\
& y(0) = 1 \quad t \in [0, 1] \\
\text{Diffusion-Reaction : } & \frac{\partial y(x, t)}{\partial t} - 0.01 \frac{\partial^2 y(x, t)}{\partial t^2} + 0.01 y(x, t)^2 - u(x) = 0 \\
& y(0, t) = 0, \quad y(1, t) = 0, \quad y(x, 0) = 0, \quad x, t \in [0, 1].
\end{aligned} \tag{9}$$

The linear ODE has been used for benchmarking optimal control solvers, for example in [27, 39, 40], and the nonlinear ODE has been used in [40, 41]. The diffusion-reaction PDE has been used as an example for the DeepXDE framework for training DeepONets [34]. We use the diffusion-reaction PDE in a tracking problem and thereby show how our method (and DeepONets) can easily be extended for more complicated optimal control problems and nonlinear PDEs.

**Network Architectures and Training.** We use the DeepONet architecture, assembling variants with minor modifications. In particular, for the linear ODE and the diffusion-reaction equation we use a standard DeepONet, while for the nonlinear ODE we use a modified DeepONet in which the fully-connected networks have been improved with residual connections as described by Wang et al. [35, 36]. The models were trained on different parameterized functions. We provide a detailed description of the network architecture, the training set, and training processes in Appendix A.

**Cost functions.** For each model, we consider three different cost functions  $J^{(p)}$ , denoted by the superscripts  $p = 1, 2, 3$ , to demonstrate the reusability of the NO. The definitions of the cost functions  $J^{(p)}$  are shown in Table 1. For the diffusion-reaction model, we solve a tracking problem, i.e., we use a squared  $L_2$ -norm for the difference between the system output  $y(x, t)$  and a reference solution  $\tilde{y}^{(p)}$ , which serves as the tracking target. The optimal control  $u(x)$  is then computed such that the system output  $y(x, t)$  closely follows this reference.

Table 1: Cost functions used for different problems.

Model	$J^{(1)}(u)$	$J^{(2)}(u)$	$J^{(3)}(u)$
Linear ODE	$\frac{1}{2} \int_0^1 (y^2 + u^2) dt$	$\int_0^1 (\frac{1}{y} + u^2) dt$	$\int_0^1 (y^4 + u^2) dt$
Nonlinear ODE	$-y(1)$	$\int_0^1 (y^2 + u^2) dt$	$\int_0^1 (y - u)^2 dt$
Diffusion-Reaction	$\ \tilde{y}^{(1)} - y\ _2^2$	$\ \tilde{y}^{(2)} - y\ _2^2$	$\ \tilde{y}^{(3)} - y\ _2^2$

Consequently, the penalized cost function minimized by the optimization routine is

$$\bar{J}_\mu^{(p)}(\{u_i\}_{i=0}^{I-1}) = \bar{J}^{(p)}(\{u_i\}_{i=0}^{I-1}) + \frac{\mu}{I} \sum_{i=0}^{I-1} \mathcal{R}_i(f, y_i, u_i, t_i) + \lambda \|\partial^2 u / \partial t^2\|_2^2, \tag{10}$$

where we have added an additional regularization term  $\|\partial^2 u / \partial t^2\|_2^2$  with a parameter  $\lambda$  to decrease oscillations in the optimized control. The norm of the second derivative is computed with a central finite difference approximation as

$$\|\partial^2 u / \partial t^2\|_2^2 = \sum_{i=1}^{m-2} (u_{i+1} - 2u_i - u_{i-1})^2. \tag{11}$$

The reduction in the oscillations around the reference solution as a result of this regularization is shown in Appendix B. For the discretization of the time vector and spatial coordinates, we use a uniformly discretized time grid with the same points as the sensor locations, that is,  $\{t_i\}_{i=0}^{I-1}$ ,  $\{x_i\}_{i=0}^{I-1}$  and  $\{u_i\}_{i=0}^{I-1}$ . This allows us to easily transform the continuous integrals to numerical integration without interpolation. We use a trapezoidal integration rule for the cost functions with integrals for numerical evaluation.

**Optimization.** We use Algorithm 1 on the regularized cost function (10) for each penalized cost function  $p = 1, 2, 3$ . Furthermore, we compare GD, ADAM and BFGS for performing the optimization step  $u \leftarrow \Phi(u, \frac{d\bar{J}_\mu}{du})$ . For starting the optimization, we use an initial guess of  $\{u_i\}_{i=0}^{I-1} = 0$  for all problems. In the BFGS method, we follow the standard of initializing the inverse Hessian as an identity matrix. For selecting appropriate optimization parameters, we perform a brief sensitivity study from which we selected parameters that provided satisfactory results across all cost functions. The sensitivity study is included in Appendix B together with the selected optimization parameters.

**Reference Solutions.** For the linear and nonlinear ODE, we solve the true solution by the direct adjoint looping together with the explicit 4<sup>th</sup>-order Runge-Kutta time integration scheme [42]. Direct adjoint looping is only suitable for optimal control problems with ODEs, and, thus, for the diffusion-reaction PDE we use the finite difference scheme provided by DeepXDE [34] to create the target  $\tilde{y}^{(p)}$  for a Gaussian random field (GRF),  $\tilde{u}^{(p)}$ , which we have randomly generated. In this way, we can create tracking targets for the diffusion-reaction problem. We use length scales  $l^{(p)}$  as 0.25, 0.35, and 0.5 for the diffusion-reaction reference control.

## 4.2 Results

The mean square error (MSE) and standard deviation (SD) of the error, computed between the solution and the reference, are summarized for all models and optimization routines in Table 2. The optimizing routine with the smallest MSE is highlighted in boldface.

Table 2: MSE ( $\pm$  SD) for different optimization methods across three cost functions

Model	Routine	Cost function $J^{(1)}$	Cost function $J^{(2)}$	Cost function $J^{(3)}$
Linear ODE	GD	1.81e-05 ( $\pm$ 4.2e-03)	1.23e-04 ( $\pm$ 1.1e-02)	5.35e-05 ( $\pm$ 7.0e-03)
	ADAM	1.73e-05 ( $\pm$ 4.0e-03)	<b>1.23e-04</b> ( $\pm$ 1.1e-02)	<b>5.35e-05</b> ( $\pm$ 7.0e-03)
	BFGS	<b>1.68e-05</b> ( $\pm$ 4.1e-03)	1.25e-04 ( $\pm$ 1.1e-02)	5.43e-05 ( $\pm$ 7.1e-03)
Nonlinear ODE	GD	1.47e-04 ( $\pm$ 1.2e-02)	2.22e-03 ( $\pm$ 4.7e-02)	8.39e-05 ( $\pm$ 8.3e-03)
	ADAM	<b>9.71e-05</b> ( $\pm$ 9.1e-03)	<b>2.16e-03</b> ( $\pm$ 4.6e-02)	<b>7.49e-05</b> ( $\pm$ 7.9e-03)
	BFGS	1.10e-04 ( $\pm$ 1.0e-02)	2.20e-03 ( $\pm$ 4.7e-02)	8.98e-05 ( $\pm$ 8.6e-03)
Diffusion-Reaction	GD	9.35e-03 ( $\pm$ 9.7e-02)	2.38e-02 ( $\pm$ 1.5e-01)	5.51e-02 ( $\pm$ 2.2e-01)
	ADAM	1.32e-02 ( $\pm$ 1.1e-01)	<b>2.35e-02</b> ( $\pm$ 1.5e-01)	<b>5.45e-02</b> ( $\pm$ 2.2e-01)
	BFGS	<b>9.26e-03</b> ( $\pm$ 9.6e-02)	2.37e-02 ( $\pm$ 1.5e-01)	5.51e-02 ( $\pm$ 2.2e-01)

**Linear ODE.** The results for the three different optimal control problems, each subject to the same linear ODE constraint, are shown in Figure 2. The top row displays the obtained optimal control using different optimization routines, while the bottom row illustrates the penalized cost value versus iteration count. All optimization routines converge to the same solution. ADAM achieves rapid convergence within a hundred iterations for all cases, despite often showing an initial increase in the cost (likely due to the hyperparameters chosen), whereas BFGS and GD converge more slowly. The obtained optimal control  $u(t)$  aligns well with the reference solution but deviates slightly from the true solution. In all cases, we observe difficulties in accurately capturing the initial and final values of the control. We suspect this issue arises partly from the enforced initial condition, which constrains the solution to a fixed value and limits the control’s influence near the initial value.

**Nonlinear ODE.** The results for the three different optimal control problems sharing the same nonlinear ODE constraint are shown in Figure 3. All methods show convergence. We observe again that ADAM converges faster than GD and BFGS, typically within a few hundred iterations or less for

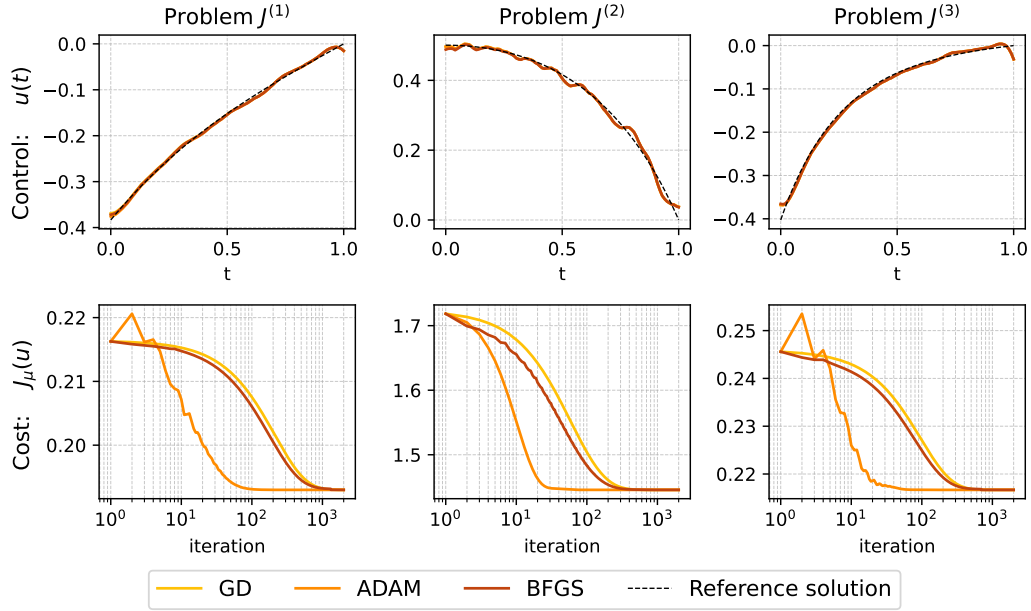


Figure 2: Results for the linear ODE with different cost functions. The top row shows the obtained control  $u(t)$  after the last iteration, while the bottom row presents the cost versus iteration. Each column corresponds to a different cost function  $J^{(p)}$ . The dotted line represents the reference solution obtained via direct adjoint looping.

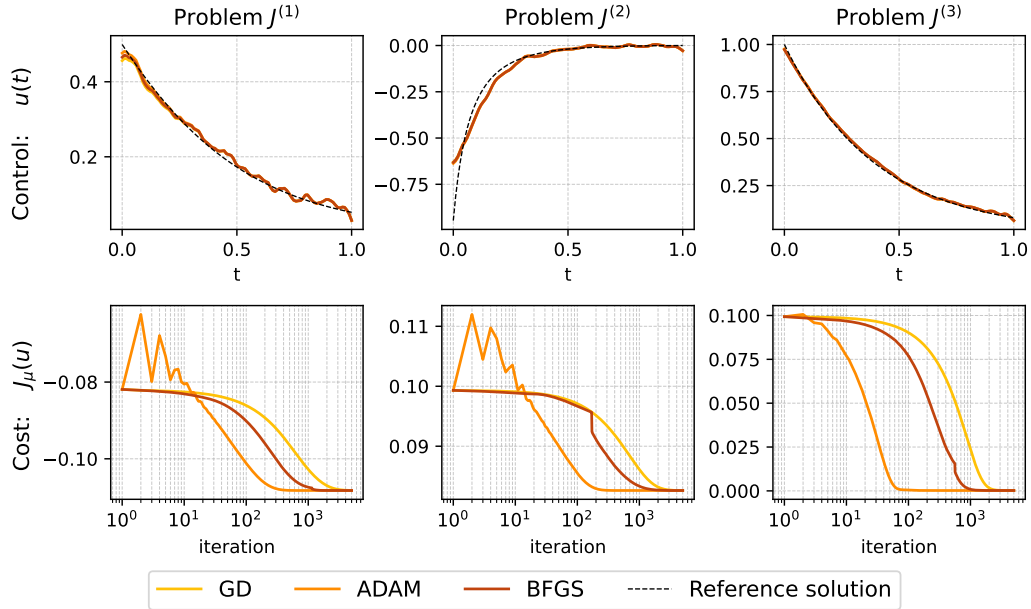


Figure 3: Results for the nonlinear ODE with different cost functions. The top row shows the obtained control  $u(t)$  after the last iteration, while the bottom row presents the cost versus iteration. Each column corresponds to a different cost function  $J^{(p)}$ . The dotted line represents the reference solution obtained via direct adjoint looping.



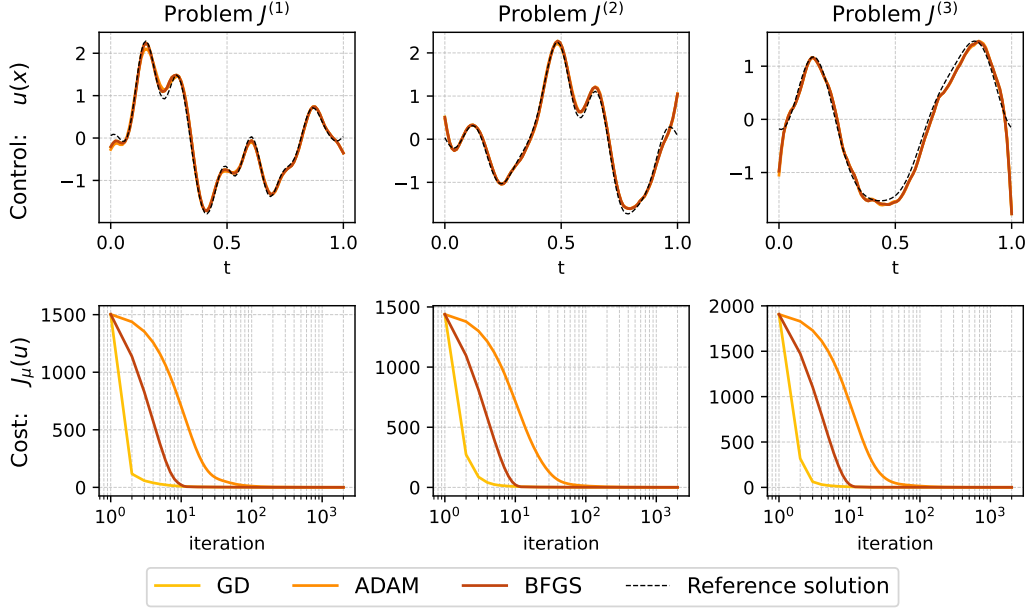


Figure 4: Results for diffusion-reaction with different cost functions. The top row shows the obtained control  $u(x)$  after the last iteration, while the bottom row presents the cost versus iteration. Each column corresponds to a different cost function  $J^{(p)}$ . The dotted line represents the reference solution which was randomly created with different length scales.

all cases. In all cases, we observe a similar deviation from the reference solution due to the enforced initial condition.

**Diffusion-Reaction** The results for the three different optimal control problems sharing the diffusion-reaction constraints are shown in Figure 3. We observe that GD, ADAM, and BFGS are capable of capturing the control  $u(x)$  and converge to the same solution. Interestingly, ADAM shows slower convergence than GD or BFGS. Similarly as for the previous cases, capturing the boundaries is difficult due to the enforced boundary conditions.

## 5 Conclusion

We demonstrated that a physics-informed DeepONet model can be directly used to solve optimal control problems without requiring any information on the cost functions during the training phase, significantly enhancing their practical applicability and reducing the architectural complexity of solving optimal control problems with neural networks. Moreover, our method demonstrated that neural operators possess capabilities that extend beyond their original role as differential equation solvers. Unlike conventional neural network approaches, we did not use control neural networks or other components to explicitly construct the solution. Instead, the trained DeepONet model was integrated into an optimization routine, where the optimal control problem was discretized, and a differential equation-based residual function was added to the cost as a penalty, ensuring that control remained in the solution space during the iterative optimization process. We computed gradients through automatic differentiation of the penalized cost function with respect to the control and used standard GD, ADAM, and BFGS optimization routines to find the optimal control.

While our study highlights the broad potential of physics-informed DeepONets for optimal control, we focused on a specific set of assumptions and settings. Our investigation was limited to the DeepONet architecture, albeit with some variations in its formulation. However, we see no limitations regarding the use of alternative architectures with likely similar or better performance, as long as they can be trained as physics-informed. We also restricted the class of admissible controls to smooth functions, which simplifies the analysis and optimization but may not capture discontinuous or

bang-bang control strategies. Finally, we assumed well-posed and bounded solution spaces, leaving the treatment of more complex or unbounded systems to future work, as well as more complicated PDEs.

### **Acknowledgments and Disclosure of Funding**

This work was supported by the Finnish Ministry of Education and Culture's Pilot for Doctoral Programmes (Pilot project Mathematics of Sensing, Imaging and Modelling).

## References

- [1] G. S. Christensen, M. E. El-Hawary, and S. A. Soliman. *Optimal Control Applications in Electric Power Systems*, volume 35 of *Mathematical Concepts and Methods in Science and Engineering*. Springer, 1987.
- [2] Roberto Caldon, Andrea Rossi Patria, and Roberto Turri. Optimal control of a distribution system with a virtual power plant. *Bulk power system dynamics and control, Cortina. d’Ampezzo, Italy*, page 18, 2004.
- [3] Maarten Steinbuch, WW De Boer, Okko H Bosgra, SAWM Peters, and Jeroen Ploeg. Optimal control of wind power plants. *Journal of Wind Engineering and Industrial Aerodynamics*, 27(1):237–246, 1988.
- [4] Banavar Sridhar, Hok K Ng, and Neil Y Chen. Aircraft trajectory optimization and contrails avoidance in the presence of winds. *Journal of Guidance, Control, and Dynamics*, 34(5):1577–1584, 2011.
- [5] Sterling J Anderson, Steven C Peters, Tom E Pilutti, and Karl Iagnemma. An optimal-control-based framework for trajectory planning, threat assessment, and semi-autonomous control of passenger vehicles in hazard avoidance scenarios. *International Journal of Vehicle Autonomous Systems*, 8(2-4):190–216, 2010.
- [6] James M Longuski, José J Guzmán, and John E Prussing. *Optimal control with aerospace applications*. Springer, 2014.
- [7] Suzanne Lenhart and John T Workman. *Optimal control applied to biological models*. Chapman and Hall/CRC, 2007.
- [8] Shuangshuang Yin, Jianhong Wu, and Pengfei Song. Optimal control by deep learning techniques and its applications on epidemic models. *Journal of Mathematical Biology*, 86(36), 2023.
- [9] Daniel Leonard and Ngo Van Long. *Optimal control theory and static optimization in economics*. Cambridge University Press, 1992.
- [10] David A Kendrick. Stochastic control for economic models: past, present and the paths ahead. *Journal of economic dynamics and control*, 29(1-2):3–30, 2005.
- [11] Saviz Mowlavi and Saleh Nabi. Optimal control of pdes using physics-informed neural networks. *Journal of Computational Physics*, 473:111731, 2023.
- [12] Deepanshu Verma, Nick Winovich, Lars Ruthotto, and Bart van Bloemen Waanders. Neural network approaches for parameterized optimal control. *arXiv preprint arXiv:2402.10033*, 2024.
- [13] Alessandro Alla, Giulia Bertaglia, and Elisa Calzola. A pinn approach for the online identification and control of unknown pdes. *arXiv preprint arXiv:2408.03456*, 2024.
- [14] Matteo Tomasetto, Andrea Manzoni, and Francesco Braghin. Real-time optimal control of high-dimensional parametrized systems by deep learning-based reduced order models. *arXiv preprint arXiv:2409.05709*, 2024.
- [15] Yongcun Song, Xiaoming Yuan, and Hangrui Yue. The admm-pinns algorithmic framework for nonsmooth pde-constrained optimization: A deep learning approach. *arXiv preprint arXiv:2302.08309*, 2023.
- [16] D.P. Kingma and J. Ba. Adam: A method for stochastic optimization. In *International Conference on Learning Representations (ICLR)*, 2015.
- [17] C.G. Broyden. The convergence of a class of double-rank minimization algorithms. *Journal of the Institute of Mathematics and Its Applications*, 6(3):222–231, 1970.
- [18] Maziar Raissi, Paris Perdikaris, and George E Karniadakis. Physics informed deep learning (part i): Data-driven solutions of nonlinear partial differential equations. *arXiv preprint arXiv:1711.10561*, 2017.
- [19] Maziar Raissi, Paris Perdikaris, and George E Karniadakis. Physics-informed neural networks: A deep learning framework for solving forward and inverse problems involving nonlinear partial differential equations. *Journal of Computational Physics*, 378:686–707, 2019.
- [20] Ameya D Jagtap, Zhiping Mao, Nikolaus Adams, and George E Karniadakis. Physics-informed neural networks for inverse problems in supersonic flows. *Journal of Computational Physics*, 448:111402, 2022.
- [21] A. Kashefi and T. Mukerji. Physics-informed pointnet: A deep learning solver for steady-state incompressible flows and thermal fields on multiple sets of irregular geometries. *Journal of Computational Physics*, 452:110904, 2022.

- [22] L. Yang, X. Meng, and G. E. Karniadakis. B-pinns: Bayesian physics-informed neural networks for forward and inverse pde problems with noisy data. *Journal of Computational Physics*, 425:109913, 2021.
- [23] Lu Lu, Raphaël Pestourie, Wenjie Yao, Zhicheng Wang, Francesc Verdugo, and Steven G. Johnson. Physics-informed neural networks with hard constraints for inverse design. *SIAM Journal on Scientific Computing*, 43(6):B1105–B1132, 2021.
- [24] Nicola Demo, Maria Strazzullo, and Gianluigi Rozza. An extended physics informed neural network for preliminary analysis of parametric optimal control problems. *Computers & Mathematics with Applications*, 143:383–396, 2023.
- [25] L. S. Pontryagin, V. G. Boltyanskii, R. V. Gamkrelidze, and E. F. Mishchenko. On the mathematical theory of optimal processes. *Doklady Akademii Nauk SSSR*, 111(5):777–778, 1956.
- [26] Pengfei Yin, Guangqiang Xiao, Kejun Tang, and Chao Yang. Aonn: An adjoint-oriented neural network method for all-at-once solutions of parametric optimal control problems. *SIAM Journal on Scientific Computing*, 46(1):C127–C153, 2024.
- [27] Enrico Schiassi, Francesco Calabrò, and Davide Elia De Falco. Pontryagin neural networks for the class of optimal control problems with integral quadratic cost. *Aerospace Research Communications*, 2:13151, 2024.
- [28] Jinjun Yong, Xianbing Luo, and Shuyu Sun. Deep multi-input and multi-output operator networks method for optimal control of pdes. *Electronic Research Archive*, 32(7):4291–4320, 2024.
- [29] Jinjun Yong, Xianbing Luo, Shuyu Sun, and Changlun Ye. Deep mixed residual method for solving PDE-constrained optimization problems. *Computers & Mathematics with Applications*, 176:510–524, 2024.
- [30] Jie Qi, Jing Zhang, and Miroslav Krstic. Neural operators for pde backstepping control of first-order hyperbolic pde with recycle and delay. *Systems & Control Letters*, 185:105714, 2024.
- [31] Rakhoon Hwang, Jae Yong Lee, Jin Young Shin, and Hyung Ju Hwang. Solving pde-constrained control problems using operator learning. In *Proceedings of the Thirty-Sixth AAAI Conference on Artificial Intelligence (AAAI-22)*, pages 4504–4512, 2022.
- [32] Lu Lu, Pengzhan Jin, Guofei Pang, Zhongqiang Zhang, and George Em Karniadakis. Learning nonlinear operators via deepnet based on the universal approximation theorem of operators. *Nature Machine Intelligence*, 3(3):218–229, 2021.
- [33] T. Chen and H. Chen. Universal approximation to nonlinear operators by neural networks with arbitrary activation functions and its application to dynamical systems. *IEEE Transactions on Neural Networks*, 6(4):911–917, 1995.
- [34] Lu Lu, Xuhui Meng, Zhiping Mao, and George Em Karniadakis. DeepXDE: A deep learning library for solving differential equations. *SIAM Review*, 63(1):208–228, 2021.
- [35] Sifan Wang, Hanwen Wang, and Paris Perdikaris. Learning the solution operator of parametric partial differential equations with physics-informed deepnets. *Science Advances*, 7(40):eabi8605, 2021.
- [36] Sifan Wang, Yujun Teng, and Paris Perdikaris. Understanding and mitigating gradient flow pathologies in physics-informed neural networks. *SIAM Journal on Scientific Computing*, 43(5):A3055–A3081, 2021.
- [37] Hans Georg Bock and Karl-Josef Plitt. A multiple shooting algorithm for direct solution of optimal control problems. *IFAC Proceedings Volumes*, 17(2):1603–1608, 1984.
- [38] Anil V Rao. A survey of numerical methods for optimal control. *Advances in the Astronautical Sciences*, 135(1):497–528, 2009.
- [39] Michael McAsey, Libin Mou, and Weimin Han. Convergence of the forward-backward sweep method in optimal control. *Computational Optimization and Applications*, 53(1):207–226, 2012.
- [40] Enkhbat Rentsen, Masaru Kamada, Amr Radwan, and Wejdan Alrashdan. A computational method on derivative variations of optimal control. *Journal of Mathematics and Computer Science*, 28:203–212, 2023.
- [41] Divya Garg, Michael Patterson, William W. Hager, Anil V. Rao, David A. Benson, and Geoffrey T. Huntington. A unified framework for the numerical solution of optimal control problems using pseudospectral methods. *Automatica*, 46(11):1843–1851, 2010.

- [42] Jacques Louis Lions. *Optimal control of systems governed by partial differential equations*, volume 170. Springer, 1971.
- [43] Adam Paszke, Sam Gross, Francisco Massa, Adam Lerer, James Bradbury, Gregory Chanan, Trevor Killeen, Zeming Lin, Natalia Gimelshein, Luca Antiga, Alban Desmaison, Andreas Kopf, Edward Yang, Zachary DeVito, Martin Raison, Alykhan Tejani, Sasank Chilamkurthy, Benoit Steiner, Lu Fang, Junjie Bai, and Soumith Chintala. Pytorch: An imperative style, high-performance deep learning library, 2019.

## A Appendix / Architectures and Training

We used a DeepONet model as a base model for our NO. The branch and trunk networks used the same architectural parameters, i.e., width, depth, etc., as shown in Table 3. For the nonlinear ODE, we used a modified fully connected (FC) network, which has a skip connection for each layer, to improve the training of the NO. The architecture for the modified FC network is presented by Wang et al.[36]. The authors refer to the model as “improved fully connected network”.

Table 3: Architectural parameters.

Parameters	Base	m	Depth	Hidden size	Activation functions
Linear ODE	FC	100	4	200	Tanh
Nonlinear ODE	Modified FC	100	5	200	Tanh
Diffusion-Reaction	FC	100	4	200	Tanh

The NOs are trained on different control function sets where the parameters for the functions are sampled uniformly from a given interval. We consider the following parameterized functions for the training set

$$\begin{aligned}
&\text{Constant : } C \\
&\text{Linear : } kt + b \\
&\text{Polynomial : } a_n t^n + a_{n-1} t^{n-1} + \dots + a_1 t + a_0 \\
&\text{Gaussian Random Field (GRF) : } \mathcal{GP}(0, \sigma^2 \exp(-\frac{|t - t'|^2}{2l^2})).
\end{aligned} \tag{12}$$

The training set is constructed of an equal number of functions drawn from a chosen subset of the types listed in (12). In addition, the parameters for each function are sampled from a uniform distribution within specific ranges. The subsets for each model and the ranges for the parameter sampling are given in Table 4. The parameter ranges were chosen to ensure that the solution of the differential equation does not exhibit excessively rapid growth or decay. As the nonlinear ODE has a quadratic term of the control  $u$ , the functions were further mapped to be in the range between  $[-1.5, 1.5]$  to avoid an uncontrollable development of the solution  $y$ . We use 100,000 functions for training the linear and nonlinear ODE models and 10,000 for the diffusion-reaction model.

Table 4: Function sets and parameter values for different problems.

Model	GRF	Polynomial		Linear		Constant
	$l$	$n$	$a_n$	$k$	$b$	$C$
Linear ODE	$[0.02, 0.5]$	$\{3, \dots, 8\}$	$[-3, 3]$	$[-2, 2]$	$[-2, 2]$	$[-3, 3]$
Nonlinear ODE	$[0.05, 0.5]$	$\{1, \dots, 5\}$	$[-3, 3]$	-	-	-
Diffusion-Reaction	$[0.02, 1.0]$	-	-	-	-	-

We trained the models purely as physics-informed, i.e., unsupervised, only based on the residual of the differential equations. We used PyTorch’s ADAM optimizer with the default parameters of  $\beta = (0.9, 0.999)$  and a learning rate scheduler that decreases the learning rate by a factor  $\gamma$  after  $n$  steps for the linear ODE. For the nonlinear ODE and the diffusion-reaction, we used constant learning rates. The hyperparameters of the training process are shown in Table 5.

Table 5: Architectural parameters.

Model	Epochs	batch size	lr	lr step size	$\gamma$
Linear ODE	1000	100	1e-4	200	0.5
Nonlinear ODE	1100	100	1e-4	-	-
Diffusion-Reaction	2500	50	1e-4	-	-

We used PyTorch [43] for the implementation. The training was performed on a standard desktop computer running an Intel Core i5-12600K processor and NVIDIA RTX A2000 GPU. The memory

usage for the model was less than a 1Gb. However, our training process was inefficient as we were not able to do a batch gradient computation for the differential equations, and had to do the batched gradient computations in a for loop. Although still manageable, this inefficiency led to high training times of approximately 10h for the linear and nonlinear ODE and 200h for the diffusion-reaction neural operator. We note that this problem can be solved, for example, in the JAX framework as shown by Wang et al. [35].

The training loss for the total (sum of all), differential equation (marked as "Physics Loss"), initial and boundary losses are shown in Figure 5. We do not monitor any test or validation set as we are not directly interested in how well the network generalizes on unseen data, but rather in whether it can solve the optimal control problem. In addition, as our training function set is quite large, thus, creating a test set that does not include any function of the training set is cumbersome and would most likely require calculating correlations between each function in the test and train sets. Hence, we deemed it to be not relevant enough to justify the effort, as the final tests are done in the optimal control framework.

In figures 6, 7, and 8, we show selected test results of the solutions for the differential equations for random GRF control functions with random length scales.

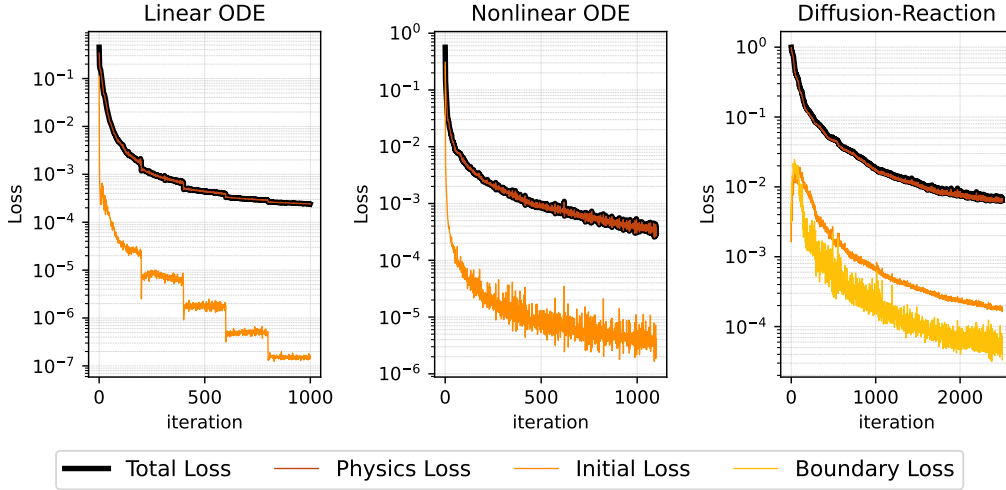


Figure 5: Training loss for the DeepONet models.

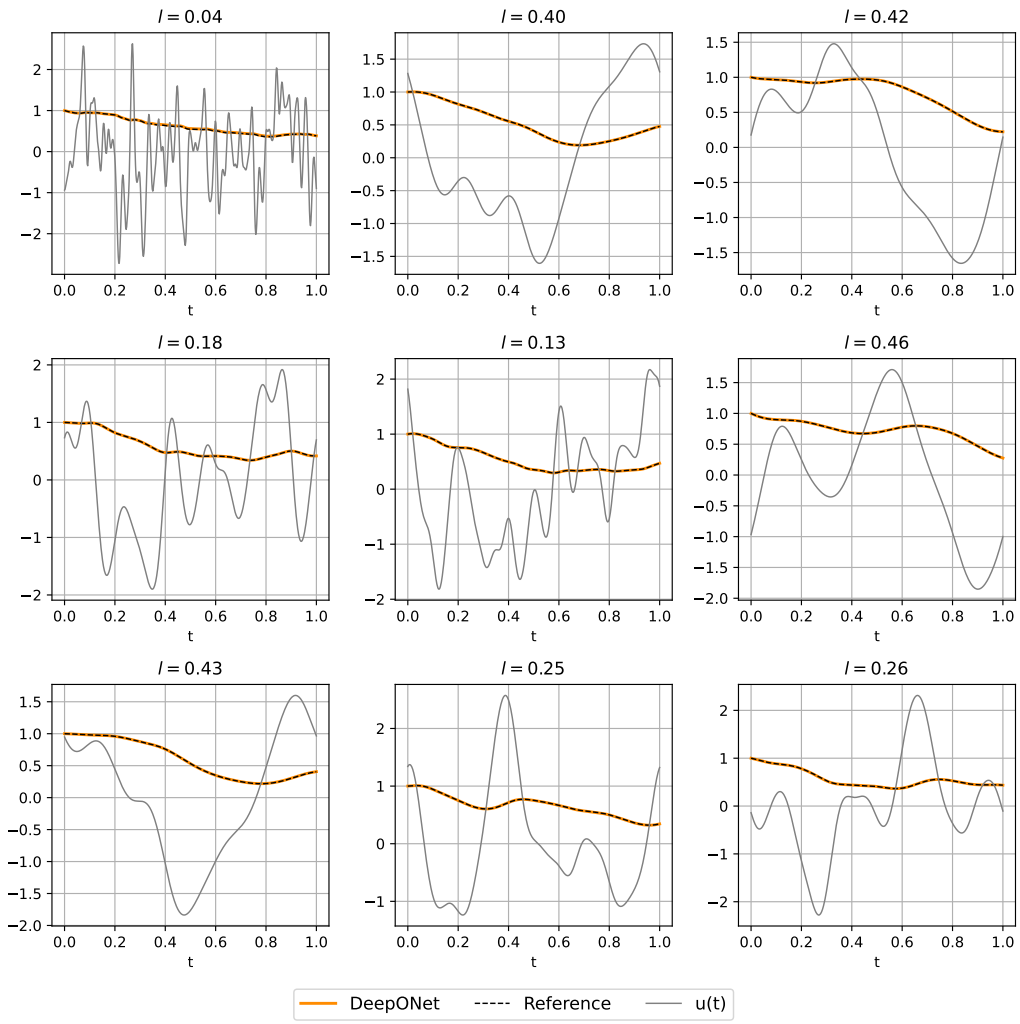


Figure 6: Random test results for the linear ode model for the GRF function with different length scales  $l$



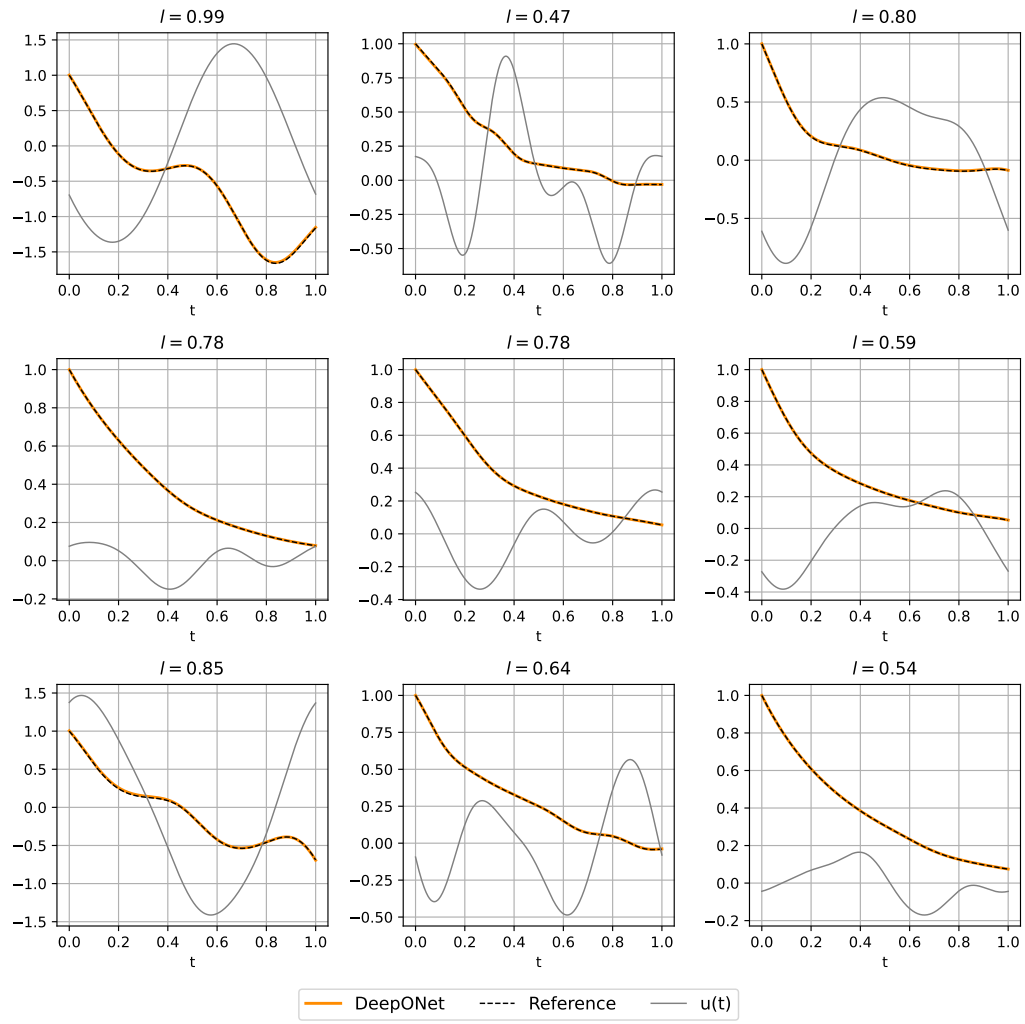


Figure 7: Random test results for the nonlinear ode model for the GRF function with different length scales  $l$

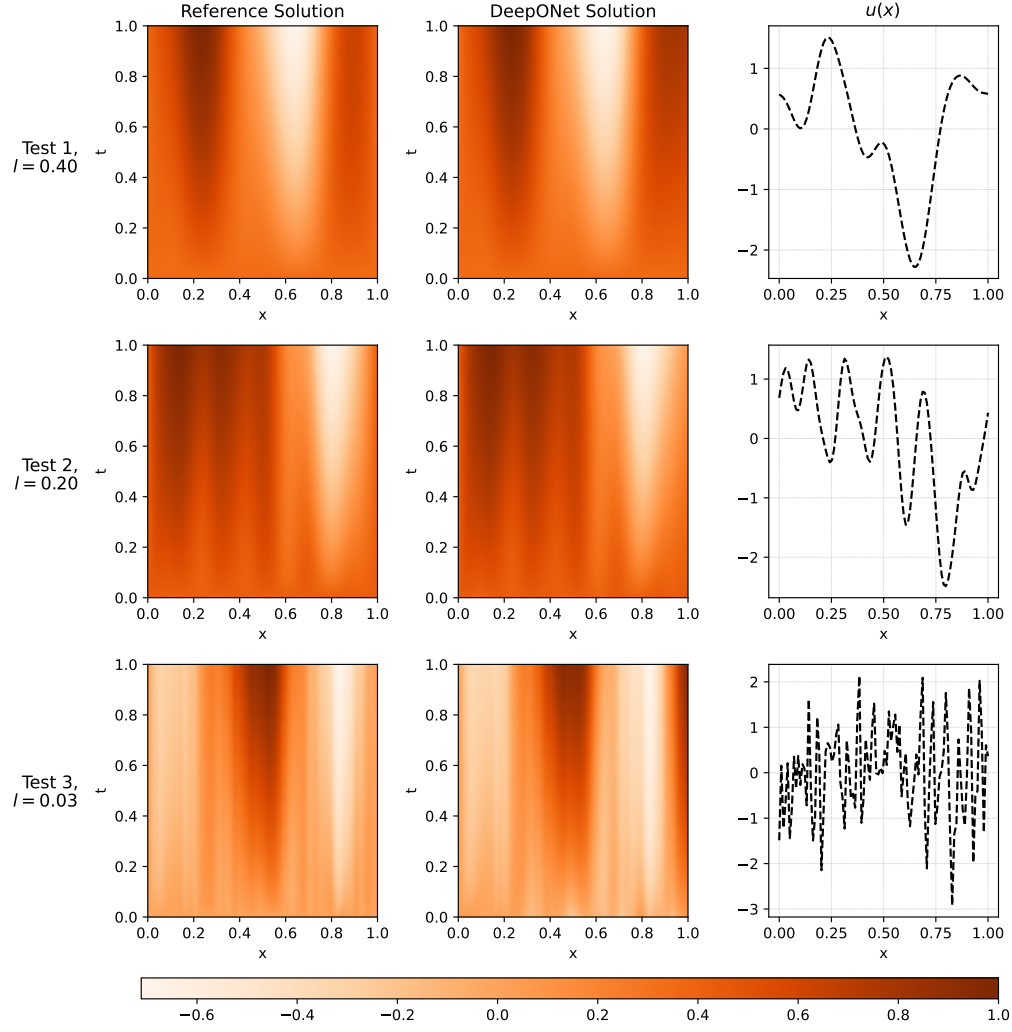


Figure 8: Random test results for the diffusion model for the GRF function with different length scales  $l$ .

## B Appendix / Sensitivity Study of Penalty and Regularization Parameters

In this appendix, we show how the penalty parameter  $\mu$  and the regularization parameter  $\lambda$  influence the solution of our method using ADAM as the optimization routine. We only used ADAM for presenting the results, as it showed the best overall performance. For this sensitivity study, we used parameter sets  $\mu = \{0, 0.1, 1, 10, 100\}$  and  $\lambda = \{0, 0.1, 1, 10\}$ . For the other optimization parameters, such as the learning rate for the step  $u \leftarrow \Phi(u, \frac{d\bar{J}}{du})$  and the amount of iterations, we observed that they do not influence the final solution as long as the learning rate is small enough so that the solutions do not diverge, but is also large enough so that the method converges with the fixed amount of iterations. Thus, we set 0.1 as the learning rate. Lastly, we used 5000 iterations for the nonlinear ODE and 2000 iterations for the linear ODE and diffusion-reaction. The results are shown for all the models and cost functions in figures 9 to 17. We use a color theme for the figures: yellow is used for the cost functions with linear ODEs, orange for nonlinear ODEs, and red for the diffusion-reaction.

The chosen parameters for the results are shown in Table 6. Note that BFGS does not require a learning rate as the step size is calculated within the routine. In BFGS, we used Armijo's rule for the line search of optimal step size with a maximum iteration of 20, with a reduction factor of 0.5 and a threshold value of  $10^{-4}$ .

Table 6: Optimization parameters.

Model	Iterations	Penalty $\mu$	Learning rate		Regularization $\lambda$
			GD	ADAM	
Linear ODE	2000	100	0.2	0.01	0.2
Nonlinear ODE	5000	20	0.1	0.01	0.2
Diffusion-Reaction	2000	20	0.02	0.02	0.5

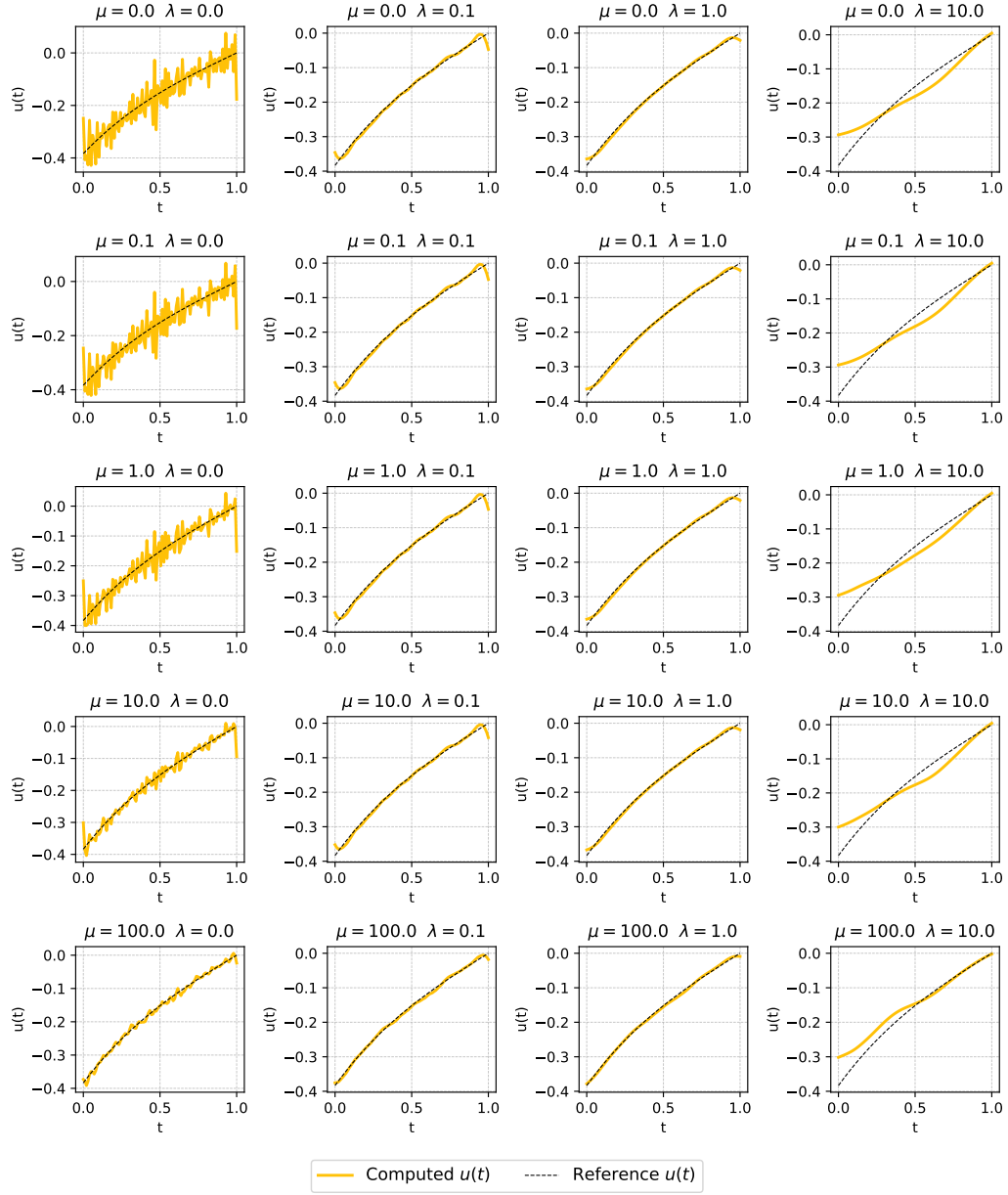


Figure 9: Sensitivity analysis for different penalty ( $\mu$ ) and regularization ( $\lambda$ ) parameters for linear ODE and cost function  $J^{(1)}$ .

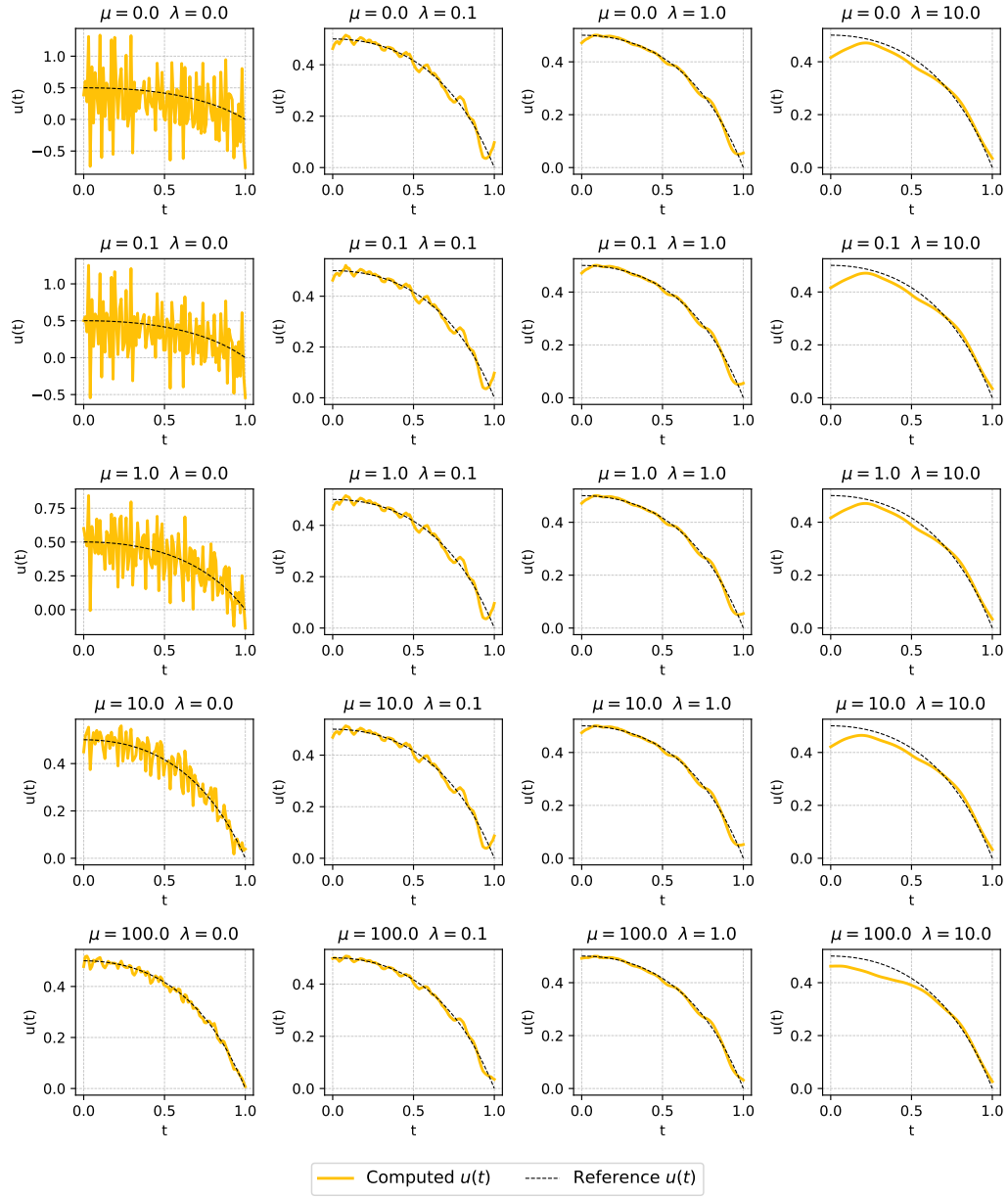


Figure 10: Sensitivity analysis for different penalty ( $\mu$ ) and regularization ( $\lambda$ ) parameters for linear ODE and cost function  $J^{(2)}$ .

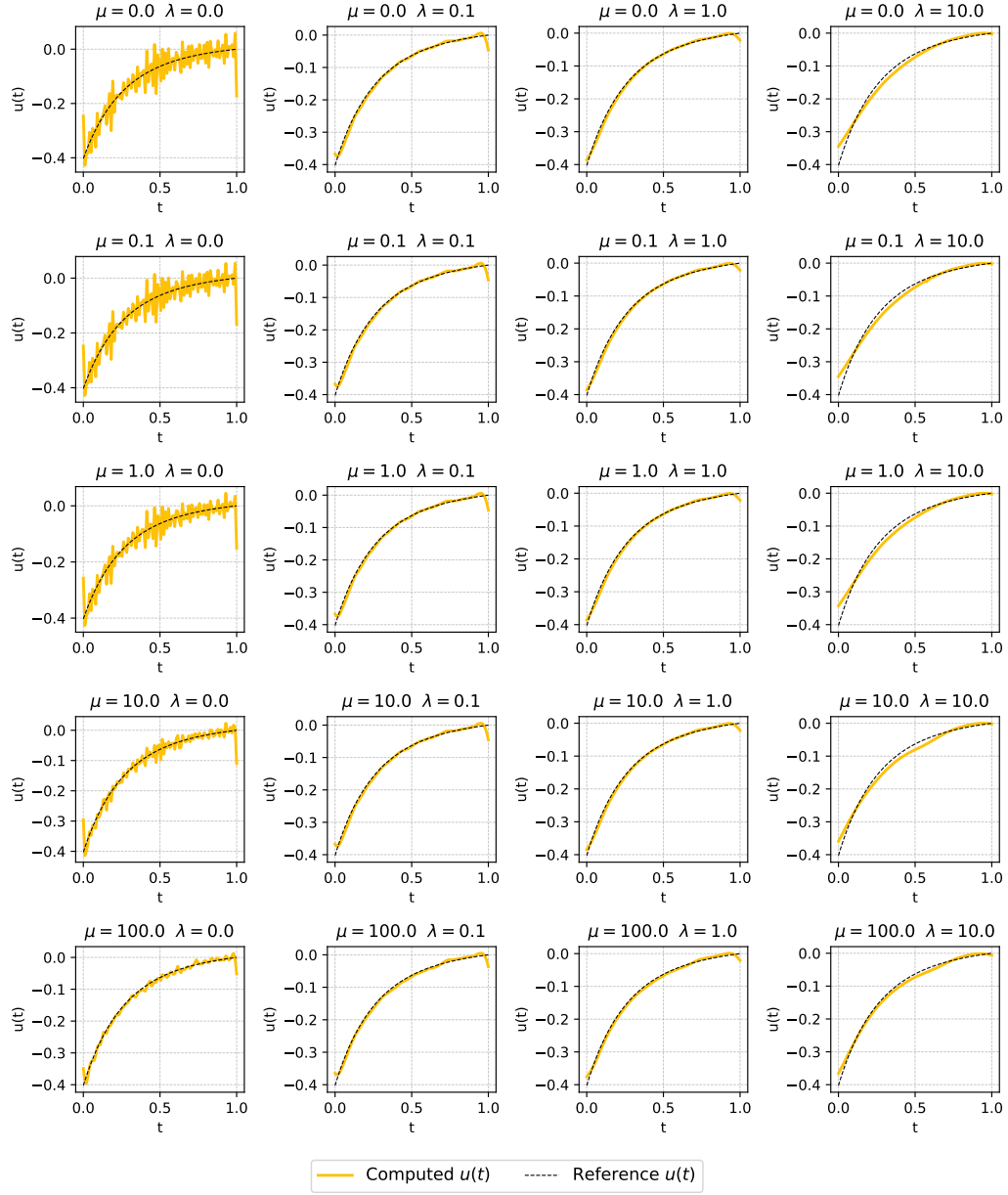


Figure 11: Sensitivity analysis for different penalty ( $\mu$ ) and regularization ( $\lambda$ ) parameters for linear ODE and cost function  $J^{(3)}$ .

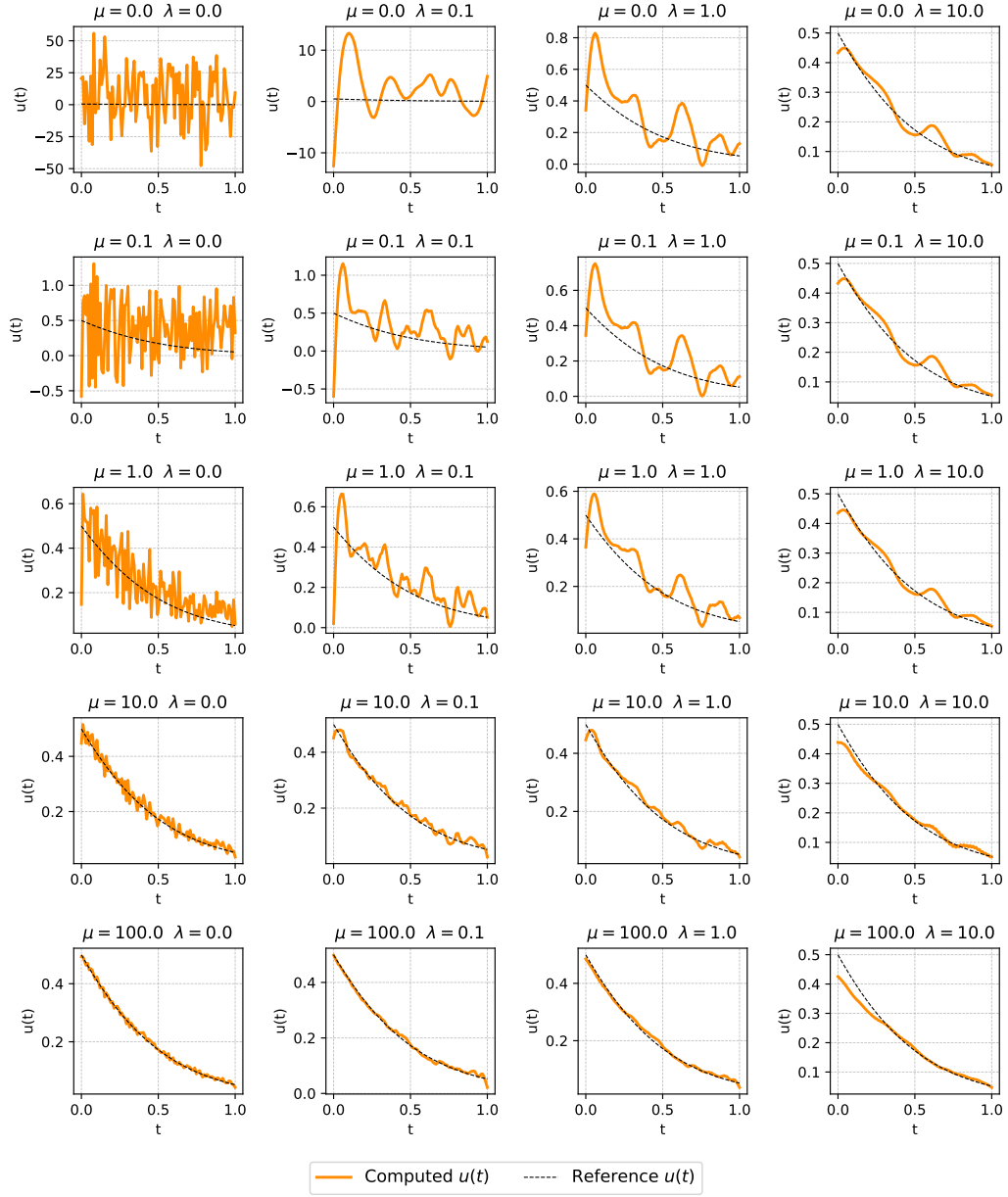


Figure 12: Sensitivity analysis for different penalty ( $\mu$ ) and regularization ( $\lambda$ ) parameters for nonlinear ODE and cost function  $J^{(1)}$ .

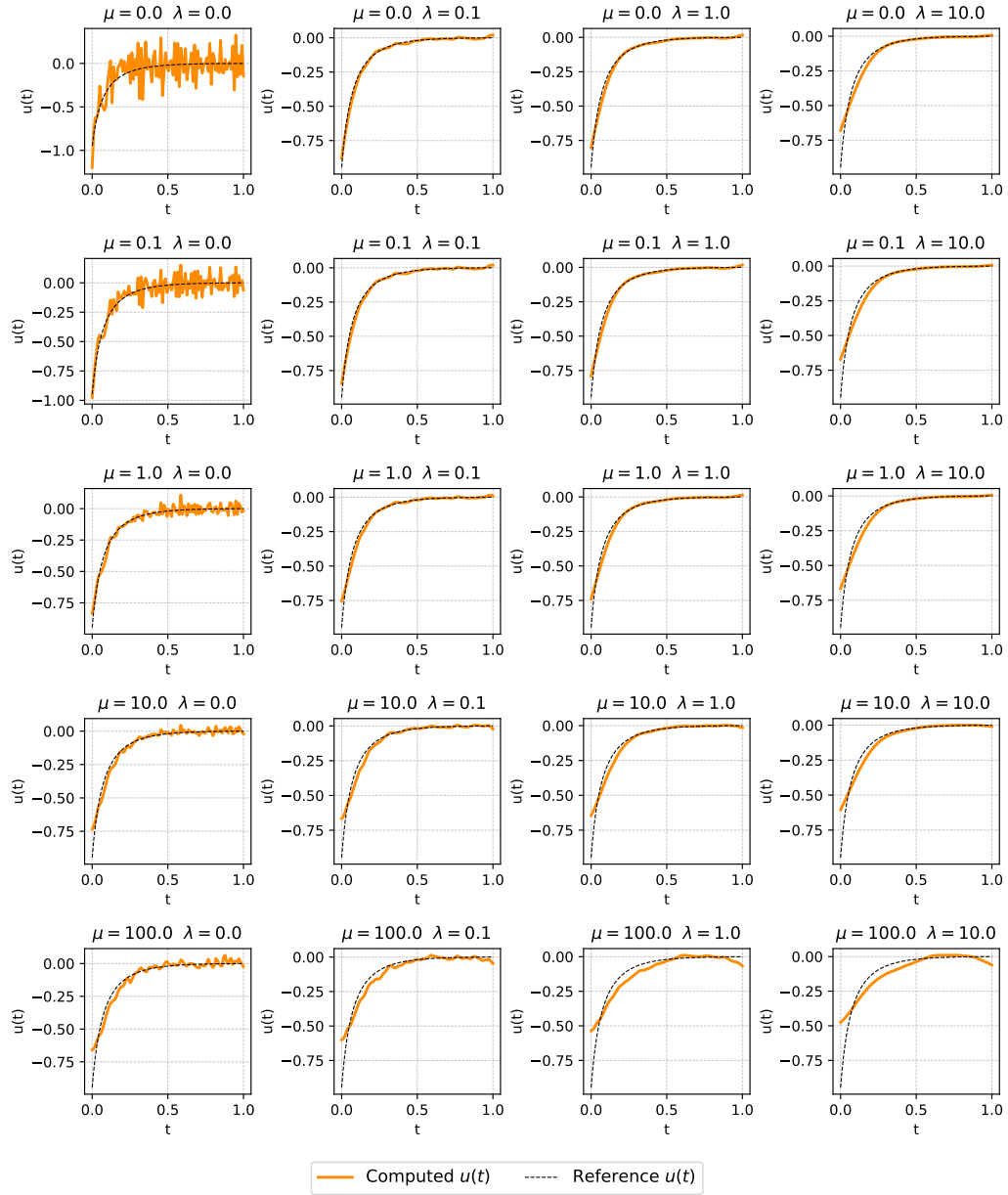


Figure 13: Sensitivity analysis for different penalty ( $\mu$ ) and regularization ( $\lambda$ ) parameters for nonlinear ODE and cost function  $J^{(2)}$ .



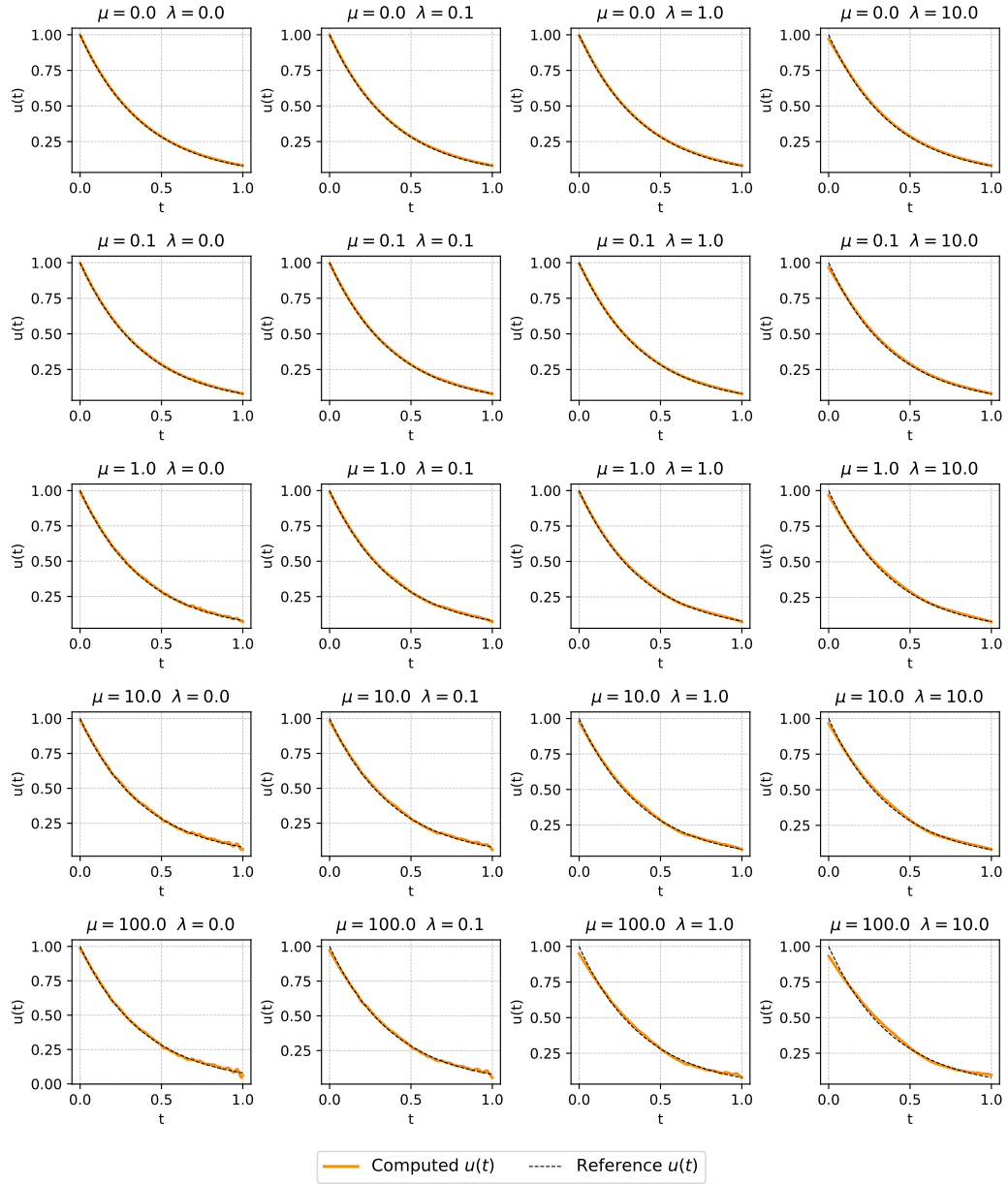


Figure 14: Sensitivity analysis for different penalty ( $\mu$ ) and regularization ( $\lambda$ ) parameters for nonlinear ODE and cost function  $J^{(3)}$ .

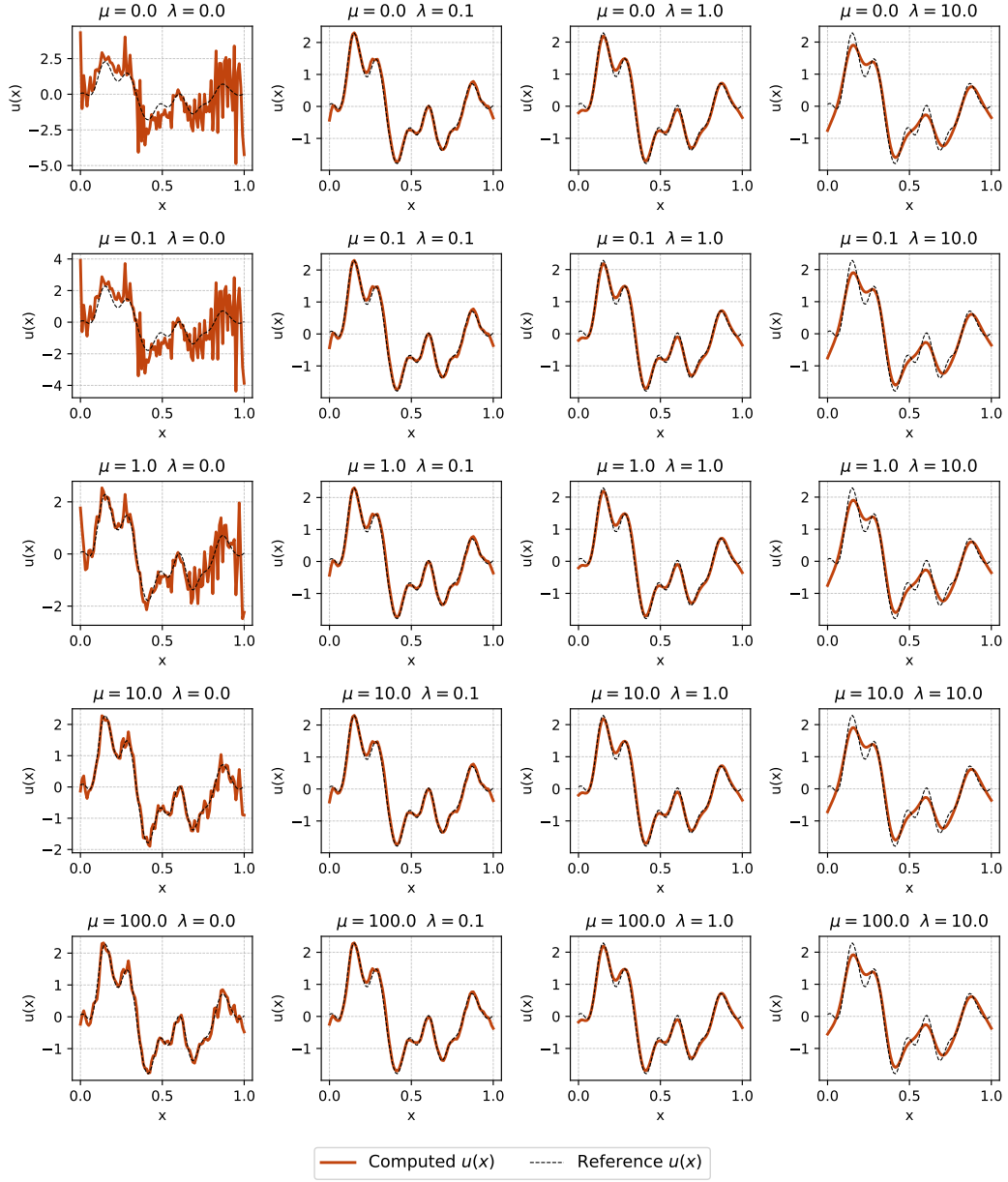


Figure 15: Sensitivity analysis for different penalty ( $\mu$ ) and regularization ( $\lambda$ ) parameters for diffusion-reaction and cost function  $J^{(1)}$ .

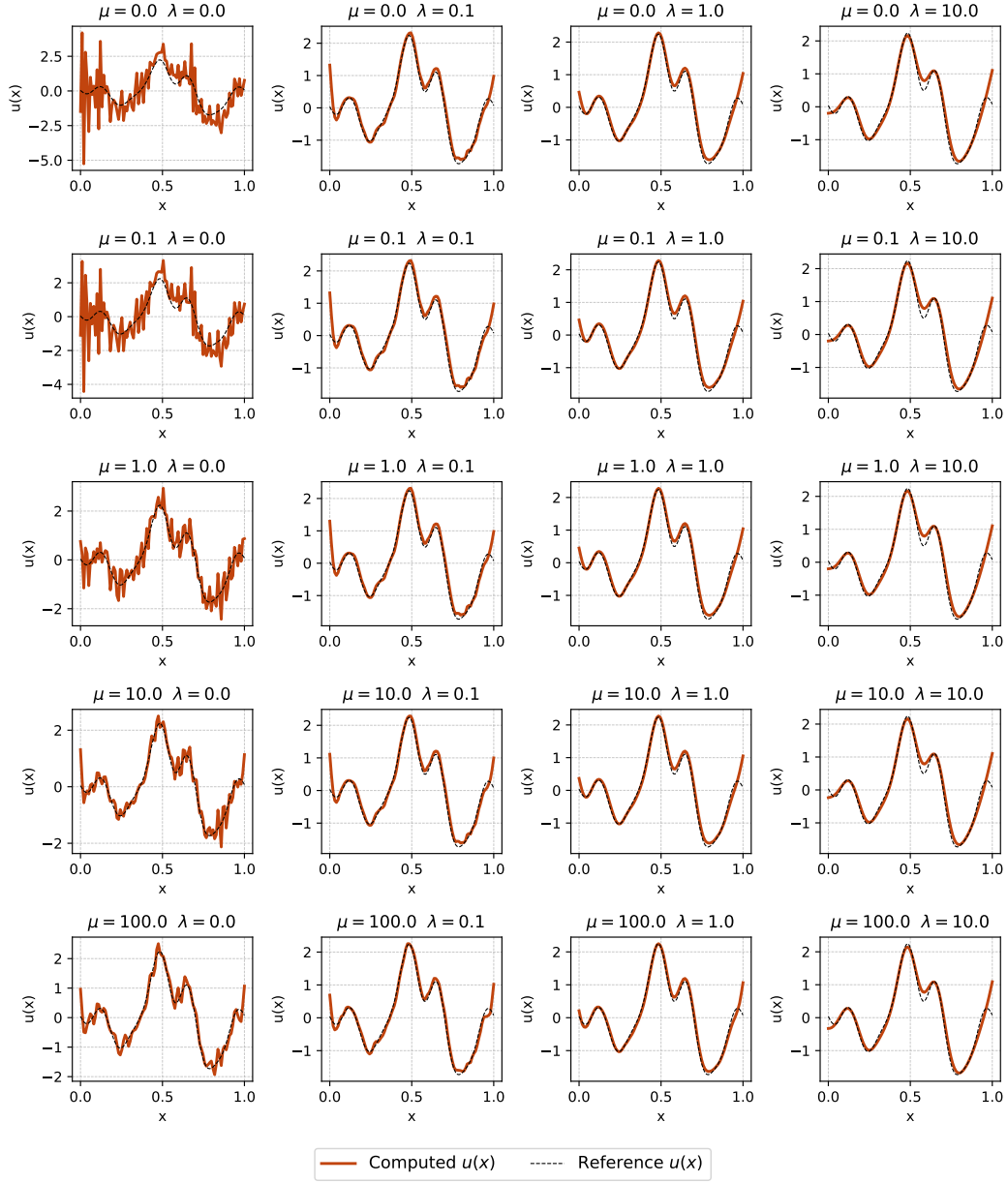


Figure 16: Sensitivity analysis for different penalty ( $\mu$ ) and regularization ( $\lambda$ ) parameters for diffusion-reaction and cost function  $J^{(2)}$ .

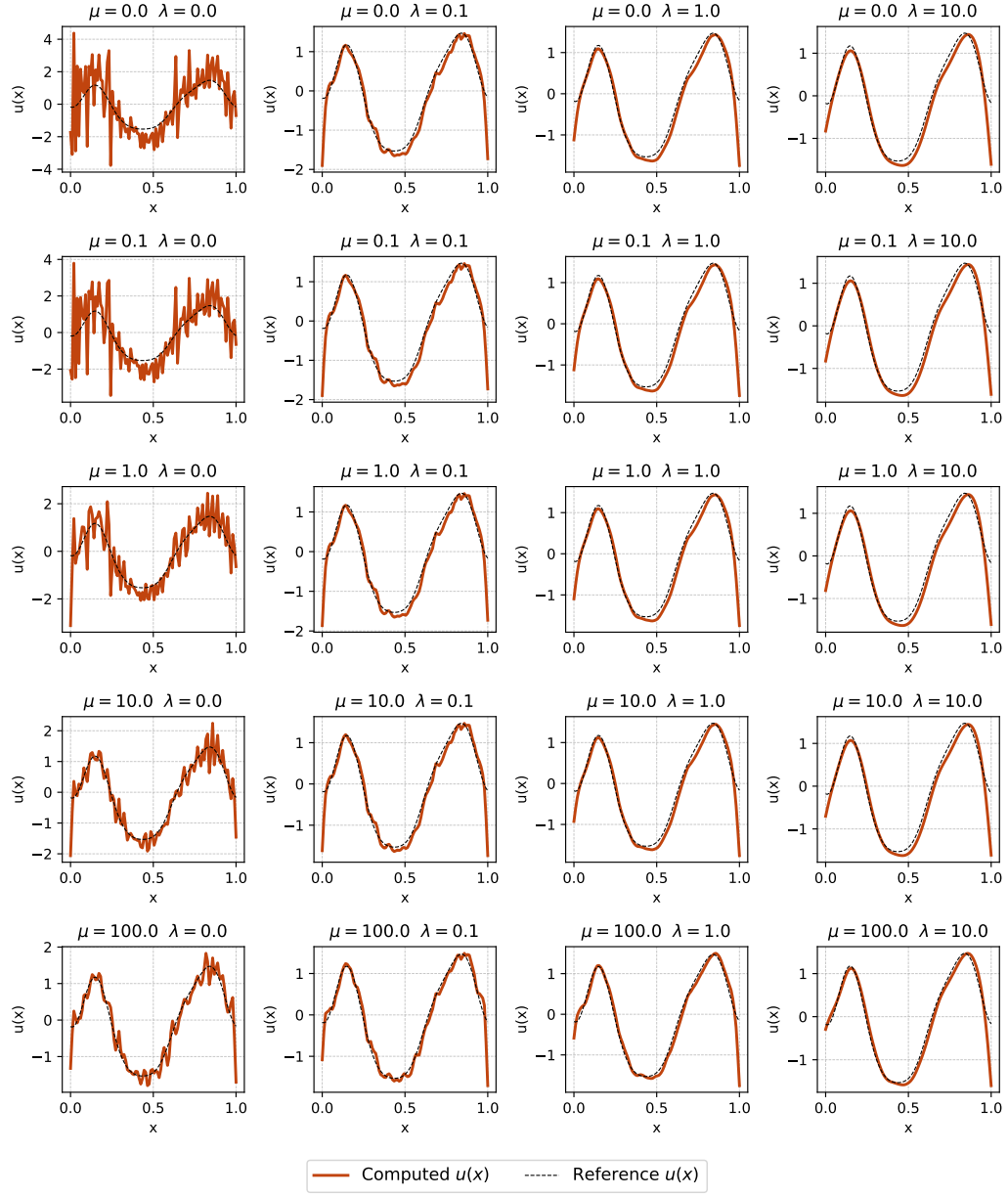


Figure 17: Sensitivity analysis for different penalty ( $\mu$ ) and regularization ( $\lambda$ ) parameters for diffusion-reaction and cost function  $J^{(3)}$ .